Egypt. J. Chem. **Vol. 64,** No. 5 pp. 2711 - 2721 (2021)

Egyptian Journal of Chemistry

http://ejchem.journals.ekb.eg/

Effect Of Poly (Aniline-Co-O-Toluidine) Loaded On Emulsion Paints With Different Pigments On Corrosion Inhibition Of Mild Steel

M. Ashraf Abdelfadeel [a]*, Ahmed I Hussain [b], Ahmed k. El-ziaty [a], Samir M. M. Morsi [b], Lobna A. Khorshed [c], S. S. Shaban [a]

[a]*Chemistry Department, Faculty of Science, Ain Shams University, Abbassia, Cairo, 11566, Egypt*

[b]*Polymers and Pigments Department, National Research Centre, Dokki, Giza, 12622, Egypt*

[c]*Physical Chemistry Department, National Research Centre, Dokki,12622, Giza, 12622, Egypt*

Abstract

Three groups of plastic emulsion paints were formulated using three different types of pigments. TiO2 was applied in the first group of paint (T-series) as a neutral pigment. Zn3(PO4)2 and Fe2O3 were added in the two other paint groups (Z-series and F-series, respectively) as anticorrosive pigments. Styrene/butyl acrylate latex was prepared by semicontinuous seeded emulsion polymerization and used as a binder in the paint formulations. Poly (ani-co-o-toluidine) (PAOT) was introduced to the painting series as an inhibitor in proportions of 0%, 1%, 2%, 3%, and 4%. PAOT inhibitor was prepared by oxidative emulsion polymerization with an equimolar amount of aniline and o-toluidine monomers. The binder and the inhibitor were tested for their particle size and chemical structure by DLS and FTIR analysis. The properties of the paint formulations were estimated physically, mechanically, and thermally. The protection efficiency of the paint coatings on steel was estimated against corrosion using an immersion test and electrochemical measurements. The DLS curves of the binder latex and the inhibitor showed a unimodal distribution of sizes 151 nm and 42 nm, respectively. However, a mix of the two emulsions exhibited a bimodal distribution of both sizes. The potentiodynamic polarization measurements showed a decrease in the corrosion current density of TiO2 coating paint from 26.4×10-7 A/cm2 to 12.3×10-7 A/cm2 in Fe2O3 coating paint. The least corrosion current density was obtained from Zn3(PO4)2 coating paint of 7.50×10-7 A/cm2. PAOT inhibitor enhanced the protection efficiency of the paint coatings with the optimum of 3%. Zn3(PO4)2 coating paint loaded with 3% PAOT inhibitor demonstrated the highest protection efficiency of 99.96%.

Key words Butyl acrylate emulsions; Poly (Ani-co-o-toluidine); Corrosion inhibition; Anticorrosion; Emulsion coatings.

1. Introduction

Day after day we are facing more difficulties regarding using metals in our daily basis, those metals can be either for personal use or what is more serious for constructions of bridges, building or even new cities. when it comes to metal it's OK, but, regarding its stability and the after-manufacturing threating it's a big deal. when metal exposed to a corrosive environment, the surface of the steel structures will corrode and thus pose a potential danger to the complete steel structure and reduce its service life [1]. We can go further in metal corrosion to reach an area where we cannot go back when metal collapse. When we talk about direct losses comes from metal corrosion, this will include replacing the damaged metal parts of the big construction which is a big waste of energy, materials and human effort. That can be fixed through repainting the bad parts of metal or the maintenance of the cathodic systems to protect metals [2, 3]. Also, excluding VOCs from paint formulation is very important since it can cause sick-building syndrome regarding the VOCs in furniture and building materials such as formaldehyde, so, treating metal surface with an anti-corrosive emulsion paint is a big deal since it based on water which is a corrodent material itself. Generally, polymers are used as insulators. However, the discovery that the organic polymers can also have conductivities comparable to

*Corresponding author e-mail: m.ashraf@sci.asu.edu.eg.; (Mohammad Ashraf).
Receive Date: 12 January 2021, Revise Date: 06 February 2021, Accept Date: 15 February 2021
DOI: 10.21608/EJCHEM.2021.57460.3239

metals and semiconductors has revolutionized this area of research especially in the electronics industry. The prospective utility of these conducting polymers or synthetic metals in electronic displays, telecommunication, electrochemical storage systems, biosensors and molecular electronics, etc., has further enhanced the interest of researchers in this important field [4-13]. Among all conductive polymers, poly anilines have been studied and grabbed great attentions because of their ease of synthesis, application and comparable high conductivity [14-21]. Designing a conductive polymer to inhibit corrosion that can outstand the high pH of paint without losing its properties and tuning it to reach its maximum electrical conductivity which is considered to be relatively high regarding metals is considered to be challenging as well. In this research we are going to synthesis a high m.wt poly (styrene-co-butyl acrylate) to be used in anti-corrosive emulsion paint formulations which will be characterized physically, mechanically, electrochemically and corrosion test.

2. Experimental

2.1. Materials

Styrene (St), butyl acrylate (BA) and acrylic acid (AA) were obtained from Sigma Aldrich, distilled before use with reduced pressure and stored at −20 °C. Acrylamide (AAm), sodium bicarbonate (NaHCO3) as a buffering agent, ammonia, potassium persulfate (KPS) were supplied from Sigma chemicals. Ammonium persulfate was obtained from Adwic Co. Ltd. Acetic acid as a doping agent was supplied by El-Nasr Pharmaceutical Chemicals Co., Aniline and o-toluidine were purchased from Merck. Sodium lauryl sulphate (SLS) as an anionic surfactant was obtained from Sigma Aldrich, cetanol as a non-ionic surfactant was obtained from BASF co., Zinc phosphate (p.s.~ 5.5 – 6 µm) was purchased from Delpahos co., red ferric oxide (p.s.~ 39.5 µm) was purchased from Toda united industrial co., titanium dioxide was purchased from Cristal co.

2.2. Methodology

2.2.1. ***Synthesis of styrene/butyl acrylate emulsion***

Styrene/butyl acrylate latex was prepared by semicontinuous seeded emulsion polymerization [22, 23]. The reaction was carried out in a 3-necked round-bottomed flask, fitted with mechanical stirrer of stainless steel, reflux condenser and two feed streams. The reactor was charged with 15 ml distilled water, emulsifier mixture of 0.4 g cetanol and 0.6 g SLS, (about ½ total amount of surfactants), 0.15 g KPS (about ⅔ total amount of initiator), and NaHCO3. The reactor was heated up to 80 oC with continuous mechanical stirring to allow the initiator to start dissociation into free radicals. The 1st feed stream is a solution mixture of monomers including 24 g styrene (0.23 mol), 26 g butyl acrylate (0.20 mol), and 2 g acrylic acid (0.027 mol). 28 ml distilled water and 1 g SDS were added to the mixture which was stirred with a high-speed homogenizer (ultra turax homogenizer) for 30 min at ambient temperature to allow the pre-emulsion process to take place. 2nd feed stream was a solution of initiator (1% wt KPS) including 0.07 g KPS dissolved in 7 ml distilled water. The 1st and 2nd feed streams were dosed to the reactor container over 3.5 h and 4 h, respectively. After which, the reaction was allowed to proceed for an additional 1 h at 80 rpm. Then, the temperature was cooled gradually to 40 oC over 1h. The pH was adjusted to 8.5 using an aqueous solution of ammonia and the product was filtered over 200-micron nylon sock. The solid content of the produced emulsion is ~ 50%. The chemical structure of the prepared styrene-acrylate copolymer is presented in Fig.1.

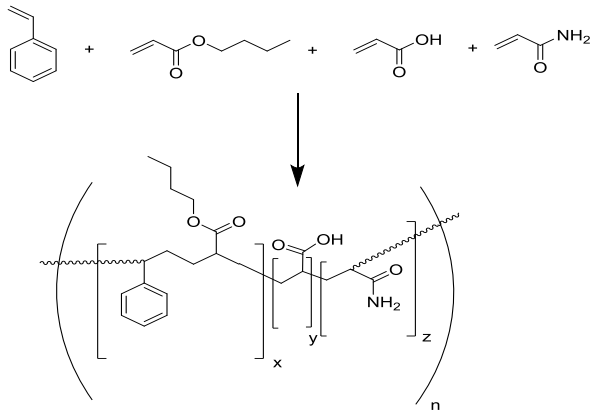

Figure.1. polymer of styrene with butyl acrylate, acrylic acid and acrylamide

2.2.2. Synthesis of poly (aniline-co-o-toluidine) emulsion

Poly (aniline-co-o-toluidine) (PAOT) was synthesized via emulsion oxidative polymerization [22, 23] using APS as an initiator, acetic acid as a doping agent, and SLS as an emulsifier. Equimolar amounts of aniline and o-toluidine monomers (0.05 mol) were fed into a three-necked flask and mixed together by a mechanical stirrer (200 rpm) at room temperature (25 oC) for 10 minutes. After that, (37.5 mmol) SLS and acetic acid (62.5 mmol) were added to

the monomers mixture and stirred at a higher speeding rate (500 rpm) for another 30 minutes. An aqueous solution of APS (0.1 M) was dropwise added using a dropping funnel with continuous stirring over 30 minutes. The reacting mixture was kept for 24 hours at room temperature and under magnetic stirring. A dark green emulsion solution of PAOT was obtained of solid content= 18%. The chemical structure of the prepared styrene-acrylate copolymer is presented in Fig. 2.

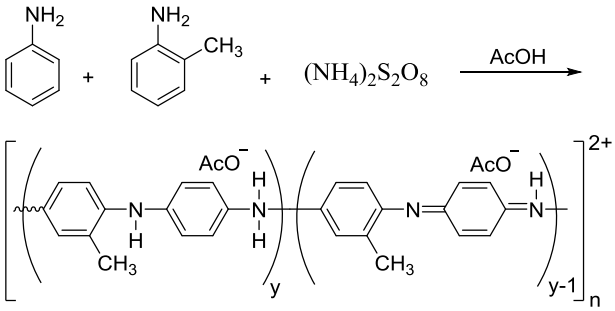

Figure 2. oxidative polymerization of PAOT

2.2.3. Paint formulation

Three series of paint formulations, T-series, Z-series, and F-series, were prepared based on TiO2 as a neutral pigment, Zn3(PO4)2, and Fe2O3 as anticorrosive pigments, respectively. The three blank paint formulations were listed in Table 1. PAOT inhibitor has been added in each formulation with a ratio of 1% - 2% - 3% - 4%. Thus, 15 paint formulas were prepared, 5 for each series, one blank and 4 with different PAOT ratios.

2.3. Characterization techniques

2.3.1. ***FTIR spectroscopy****:* Fourier transform infrared (FTIR) spectra of the prepared samples were recorded by JASCO FTIR 6100 in the range of 4000–400 cm-1 with 4 cm-1 resolution and 50 scans with a scanning speed 2mm/sec.

2.3.2. ***DSC analysis***: Differential scanning calorimetry analysis (DSC) was recorded on TA Instruments DSC Q20 V24, 11 Build 124. All samples were heated with a scan rate of 10 oC/min over a *temperature range of -10 to 500 °C under a nitrogen atmosphere.*

2.3.3. ***DLS analysis****:* The size of latexes particles and their distribution were determined by dynamic light scattering (DLS) in the range of 0.4–500 nm using Malvern Zetasizer nano, UK. The emulsions were diluted with water in a plastic cuvette before measurement. The particle sizes and zeta potentials were given as an average of three measurements.

Table 1. Paint formulations of the three blanks of T-Z-F-series.

Ingredients	**Weight (g)**
Water	287
Propylene glycol	37
Acrylic thickener	3
Antifoaming agent	3
Dispex® A40	3
Mergal® 395	2
TiO_2	70
Talc	180
TiO_2 (T-series) or $Zn_3(PO4)_2$ (Z-series) or Fe_2O_3 (F-series)	100
Styrene/acrylic emulsion	300
Texanol	10
Triethanol amine	3
Ammonia solution	2
Total	**1000**

2.3.4. ***Physical and mechanical tests***: The viscosity was measured according to ASTM D2196-10, 2010 using a digital viscometer manufactured by Sheen Company. The solid content (S.C.) was calculated as the average of three experiments according to ASTM D4209-07, 2013.

$$S.C. = \frac{W_i}{W_o} \times 100$$

where Wi is the final weight of the sample after drying and Wo is the initial weight of the sample.

2.3.5. ***Hardness test***: The prepared coating formulations were applied on metal or glass panels by using a film applicator to obtain an appropriate and uniform dry film thickness. The scratch hardness of the prepared dry films was estimated by using pencil hardness tester according to ASTM D3363-05, 2011.

2.3.6. ***Bending test***: The bending of the prepared dry films was measured by cylindrical mandrel bending tester according to ASTM D522-08, 2008. The dried films, coated on tin plates, were bent over a cylindrical mandrel of different mm diameter and the resistance to cracking of the coatings was determined.

2.3.7. ***Visual corrosion test:*** Paint formulations were then applied to well cleaned steel panels (5 × 7 cm^2

area) using a film applicator of 200 microns and left to dry for 10 days. After complete dryness, the edges of the steel panels were covered with a thick layer of epoxy paint to protect edges from corrosion. The coated faces were scratched with a sharp blade to about 1-mm width to expose the bare metal. The panels were then exposed to artificial seawater (3.5 wt% NaCl solution) for 28 days. At the end of this time the panels were visually evaluated for the degree of rusting and degree of blistering according to ASTM D 610–08, 2012 and ASTM D 714–02, 2009, respectively.

2.3.8. ***Potentiodynamic polarization measurements:*** The potentiodynamic polarization test was carried out by workstation Autolab PGSTAT302N – High-Performance potentiostat/galvanostat instrument. Three conventional electrode cells; a working mild steel electrode, a platinum counter electrode, and a reference Ag/AgCl electrode, were immersed in 3.5 % NaCl as an aggressive solution at room temperature. Tafel curves or potentiodynamic polarization curves of bare and coated mild steels were measured from steady-state potential ±250 mV at a scan rate of 2 mVs^{-1}. Corrosion rate information was obtained by the extrapolation of the Tafel plots which provides the cathodic and anodic polarization curves of the corrosion processes. Extrapolation of these curves to their point of intersection provides both the corrosion potential and the corrosion current density. The electrochemical parameters were estimated as follows:

Corrosion current (Icorr) in amperes/cm2 was given according to Stern-Geary equation (1) [22, 24]

$$I_{corr} = \frac{1}{R_p} \frac{\beta a \beta c}{2.303\,(\beta a + \beta c)} \quad \ldots\ldots\ldots\ldots\ldots\ldots\ldots\ldots (1)$$

where Rp is the polarization resistance in ohm.cm2, βa and βc are the anodic and cathodic tafels slopes in volts/decade, respectively.

Corrosion rate (CR) in millimeters per year (mm/y) was calculated from Faraday's law equation (2) [22, 25, 26]

$$CR = \frac{I_{corr}\, K.\, EW}{dA} \quad \ldots\ldots\ldots\ldots\ldots\ldots\ldots\ldots (2)$$

where K is a constant that defines the units of corrosion rate and equals to 3272 mm/y, EW is the equivalent weight in grams/equivalent, d is the density in g/cm3, A is sample area in cm2.

The coating efficiency (η%) was calculated according to equation (3) [25, 27]

$$\eta\,\% = \frac{I_{corr} - I^{o}_{corr}}{I_{corr}} \times 100 \quad \ldots\ldots\ldots\ldots\ldots\ldots\ldots\ldots (3)$$

where Icorr and $I^{o}corr$ are the corrosion currents in the absence and the presence of the coating, respectively.

3. Results and discussion

3.1. FTIR and DSC analysis of styrene/butyl acrylate emulsion

The chemical structure of the prepared styrene/butyl acrylate copolymer emulsion was presented in Figure 1. The FTIR spectrum of the copolymer is shown in Figure 3. The bands at 3027 to 3079 and 1501 cm-1 are assigned to =C–H and C=C aromatic rings stretch of styrene moieties, respectively. However, the bands at 692, 752 and 835 cm-1 are attributed to aromatic ring puckering. The strong and broad band at 1726 cm-1 is related to the carbonyl stretching of O=C–NH2 (acrylamide), O=C–OH (acrylic acid), and O=C–O– (butyl acrylate). The C–O and C-N stretching vibrations appeared as two bands at 1245 and 1162 cm-1, respectively [22, 28]. The N–H stretching of acrylamide is clearly observed at 3438 cm-1. CH2 asymmetric and symmetric vibrations appeared at 2925 and 2854 cm-1, respectively. The broad band from 2500 to 3500 cm-1 is related to O–H stretching of acrylic acid carboxylic groups.

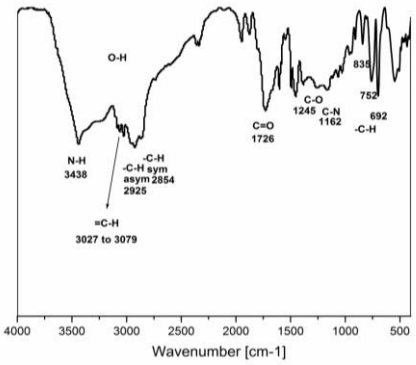

Figure 3. FTIR spectrum of the prepared styrene/butyl acrylate copolymer emulsion.

Figure 4. shows the particle size distribution curve of the synthesized styrene/butyl acrylate copolymer emulsion. The curve exhibited a unimodal pattern of size ~ 151 nm indicating the uniformity of the particles in the latexes. The zeta potential value of prepared copolymer emulsion was determined to be -41 mV. This value indicates the good stability of the emulsified particles within the aqueous medium. The negative sign of PSBAA latexes is assigned to the

anionic surfactant and carboxylate ions of acrylic acid that electrostatically stabilize the colloid.

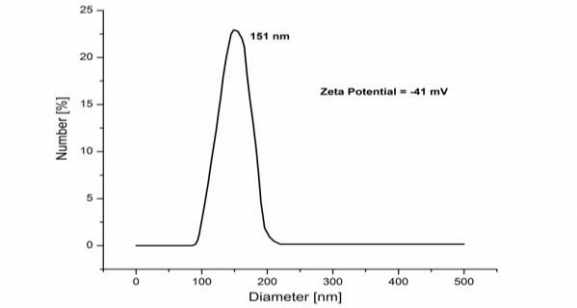

Figure 4. Particle size distribution curve and zeta potential value of the prepared styrene/butyl acrylate copolymer emulsion.

3.2. FTIR analysis of poly (aniline-co-o-toluidine) emulsion

The chemical structure of the prepared PAOT emulsion was presented in Figure 4. The FTIR spectrum of the PAOT is shown in Figure 5. The characteristic peak about 3438 cm–1 corresponds to the N-H stretching of the primary amine and confirms the amino group. The peaks at 2925 cm–1 and 2854 cm–1 attribute to the C-H stretching vibration of methyl group. The absorption peak at 1573 cm–1 is assigned to the quinoid ring stretching. The peak observed at 1470 cm–1 corresponds to the presence of C=C stretching vibration in benzenoid ring [26, 29, 30]. The sharp peak at 815 cm–1 attributes the para-coupled phenyl ring in the copolymer. The absorption band around 1111 cm–1 confirms the charge delocalization. The peak at 1215 cm–1 corresponds to the C-N stretching vibrations of the aromatic primary amine.

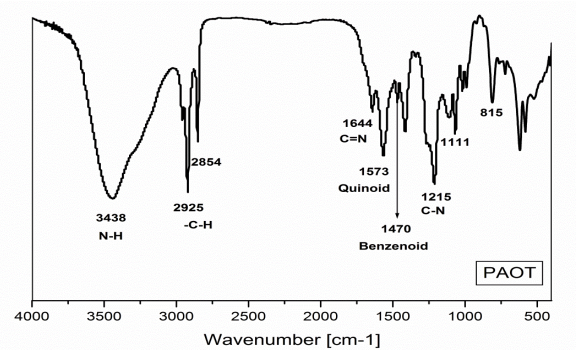

Figure 5. FTIR spectrum of the prepared PAOT copolymer emulsion.

3.3. *Physical and mechanical properties of the paint formulations*

Table 2 lists the physicomechanical properties of the paint films which are affected by the pigments and the chemical composition of the binder. The viscosity and density decreased gradually with increasing the amount of PAOT emulsion added in the paint formulations. This is due to the low solid content of PAOT emulsion (18%) which led to the reduction of viscosity and density of the paint formulations. Z-series exhibited higher hardness than T-series, this may be due to the integration of $Zn_3(PO_4)_2$ anticorrosive pigment to the coated paint formulations which increases hardness than in case of titanium dioxide. Also, a relatively higher hardness values in case of F-series maybe attributed to the higher hardness of Fe2O3 particles. Also, in the three series, the incorporation of PAOT into the paint formulations increased the hardness of the coating films. This is because, according to the results obtained from the DSC curves, PAOT enhanced the physical interactions between the polymeric chains. The flexibility of the paint films was preserved with the variation in both the

Table 2. Physical and mechanical properties of the paint formulations.

Sample Code	Bending Test	Density (g/cm^3)	Viscosity (cp)	Hardness Test	Adhesion Test
T0	1mL	1.35	815	6B	1B
T1	1mL	1.32	1102	4B	3B
T2	1mL	1.3	1050	4B	3B
T3	1mL	1.25	955	2B	4B
T4	1mL	1.22	802	B	4B
Z0	1mL	1.336	895	4B	3B
Z1	1mL	1.3	1190	4B	3B
Z2	1mL	1.27	1008	B	3B
Z3	1mL	1.21	810	H	4B
Z4	1mL	1.15	799	F	4B
F0	1mL	1.4	1411	B	3B
F1	1mL	1.38	1489	HB	4B
F2	1mL	1.33	1405	HB	4B
F3	1mL	1.28	1325	F	4B
F4	1mL	1.25	1303	H	4B

pigments used and the amount of PAOT in the paint formulations.

3.4. Thermal characteristic of the paint formulations

DSC analysis was performed to study the effects of the neutral and anticorrosive pigments and the PAOT inhibitor on the thermal properties of the paint coatings. Figures 6, 7, and 8 show the DSC curves of the styrene/acrylate copolymer with T0 and T3 (Figure 6), Z0 and Z3 (Figure 7), and F0 and F3 (Figure 8). For the copolymer, a clear endothermic peak appeared at 22oC and related to the glass transition temperature (Tg) of the copolymer film. Two other degradation endotherms at 316oC and 368oC which may be related to decomposition of functional groups (amide, ester, and acid) and backbone chains, respectively. Whereas, after adding the pigment to the polymer, we notice that the glass transition temperature increased from 22oC to 25oC, for TiO2, 28oC, for Fe2O3, and 33oC, for Zn3(PO4)2. Also, other shifts to higher values are observed in the endothermic degradation curves illustrated in the figures. This is due to some complexes and chelation formed between the metals and the functional groups in the polymer chains. While the addition of the inhibitor to the formulations led to a further increase in the glass transition temperatures of their films to 28oC, for TiO2, 30oC, for Fe2O3, and 36oC, for Zn3(PO4)2. Additional increase in the final degradation temperature by 10oC to 12oC compared with TiO2, Fe2O3, and Zn3(PO4)2 films. An additional endothermic peak appeared at 240 oC – 247 oC due to decomposition of the dopant. However, the degradation peak of the amide, ester, and acid of the copolymer, which emerged at 316 oC in the neat copolymer and at 325 oC to 335 oC for the pigmented copolymer, appeared as a broad shoulder combined with the main degradation peak of the copolymer backbone. This shoulder is related to, in addition to the functional groups decomposition of the copolymer, the degradation of the oligomers of the inhibitor. The latter contributed in additional physical interactions with the copolymer chains and complexation with the metallic pigments. This is indicated by the elevated thermal stability and Tg values of the films filled with the inhibitor.

Figure 9a and 9b. shows the different effect of the pigments on the physical interactions originated between the copolymer and the inhibitor with the pigment. Zn3(PO4)2 contributed in the highest physical interactions followed by Fe2O3 and the least is TiO2. This may be due to the more chelations originated between the Zn metals and the lone pair of electrons on the floating on the polar groups along the copolymer chains and the aromatic rings of the inhibitor. Moreover, the oxygen atoms in the phosphate group interred in hydrogen bonds with the polar groups of the copolymer.

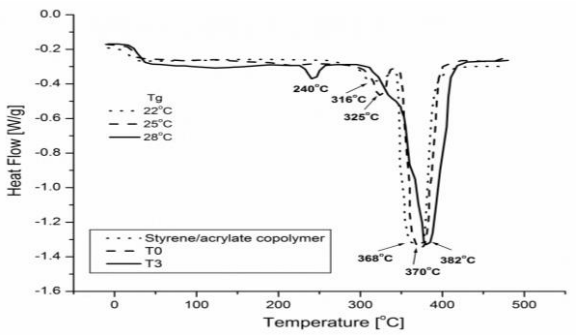

Figure 6. DSC curves of the prepared styrene/acrylate copolymer, T0, and T3.

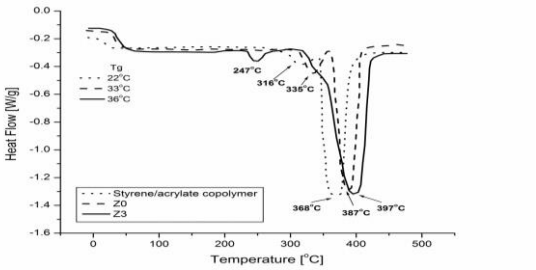

Figure 7. DSC curves of the prepared styrene/acrylate copolymer, Z0, and Z3.

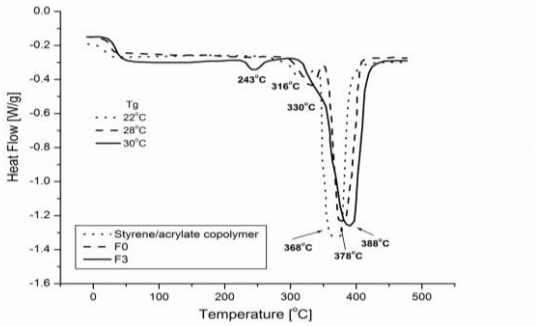

Figure 8. DSC curves of the prepared styrene/acrylate copolymer, F0, and F3.

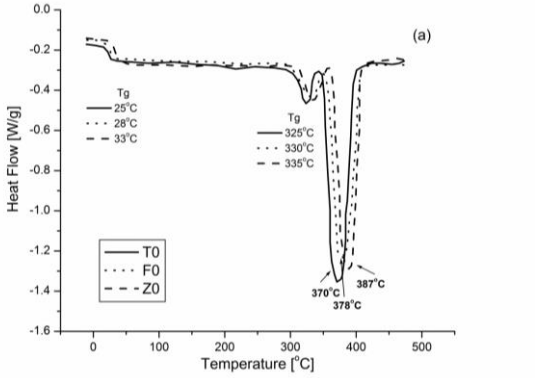

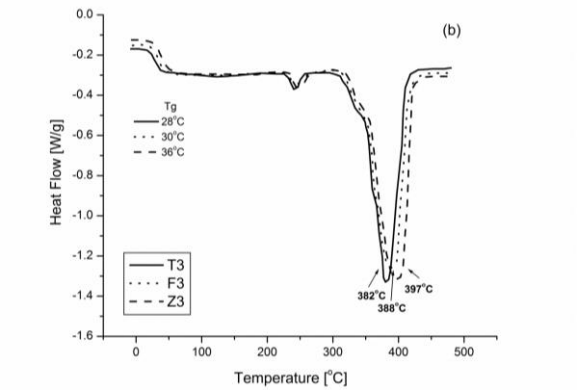

Figure 9. DSC curves of T0, Z0, and F0 (a) and T3, Z3, and F3 (b).

3.5. Corrosion testing

3.5.1. Immersion test

Figure 10 presents the steel panels coated by the paint formulations with and without PAOT after immersion in 3.5% NaCl salt solution for 28 days. Table 3 indicates the rusting and blistering degrees of the tested coated mild steel samples after 28 days of immersion. T0-coated steel panel showed a high degree of rusting and some blisters in the coat. Loading paint with 10% anticorrosive pigments, zinc phosphate and red iron oxide in Z and F series respectively improved the protection efficiency of the coatings (Z0 and F0). Steel panels coated with T3 and T4 exhibited the lowest degree of rusting in T-series. The protection efficiency increased with increasing PAOT loaded in the formulations up to 3% and 4%. This is due to increased current dispersion effect resulting from high conjugation property of PAOT as a highly conductive polymer to reach its maximum in case of T3 and T4 paint films on the substrate as illustrated in Table 3. As mentioned before where Z- and F-series showing a good elevation in corrosion inhibition efficiency when compared with T-series. Z3, Z4, F3 and F4 showed the best coat efficiency. Bigger particle size of red ferric oxide than of zinc phosphate made F-series more liquid permeable leading to increase the pores size of the F-series coats causing denser blisters and hence, lower corrosion resistance as shown below.

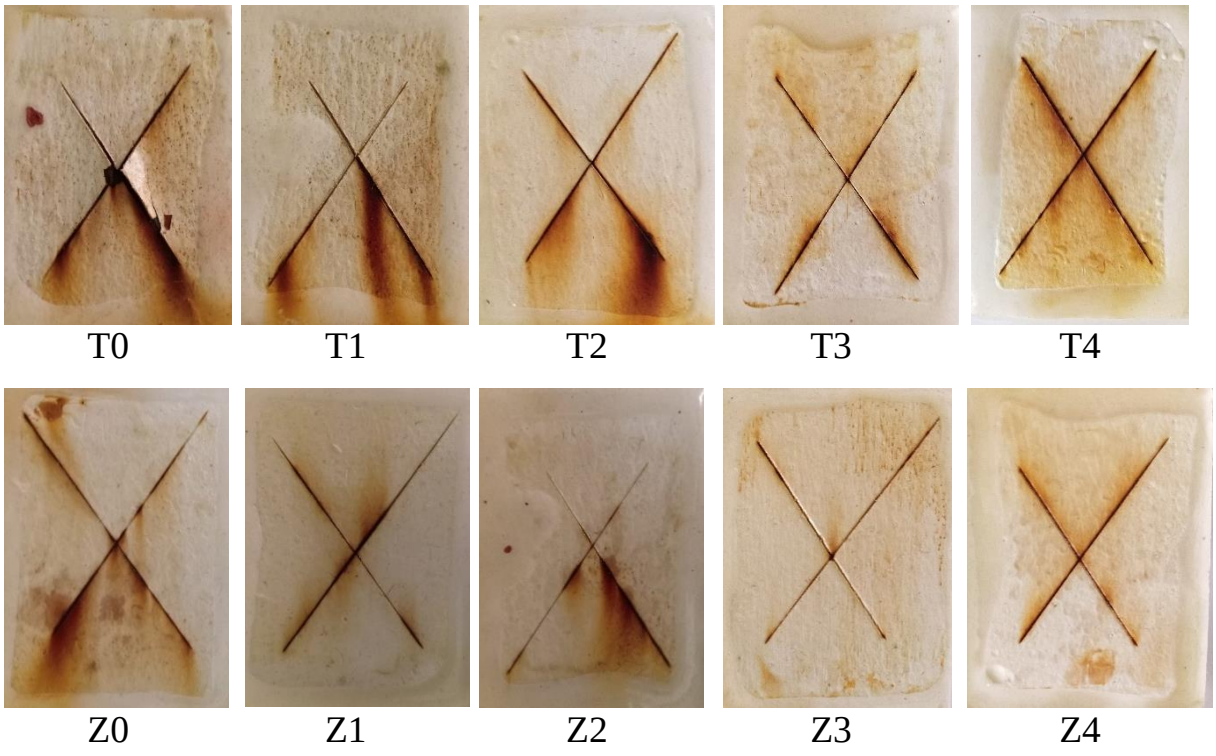

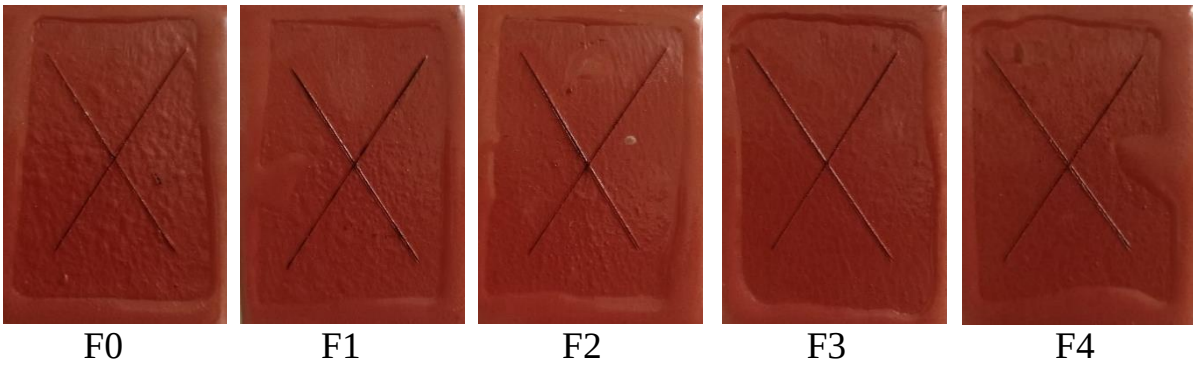

Figure 10. Corrosion test photos of coated panels after 28 days of immersion in 3.5% NaCl solution.

Table 3. Corrosion test evaluation of the paint films after immersion in 3.5% NaCl salt solution for 28 days

Sample Code	Corrosion test evaluation		
	Degree of Blistering	Degree of rusting	Failure at the scribe
T0	2F	1	5
T1	2M	2	7
T2	4F	2	7
T3	2F	3	8
T4	4F	2	8
Z0	2F	2	9
Z1	4F	2	9
Z2	4F	4	9
Z3	4F	5	10
Z4	4F	4	10
F0	2D	2	8
F1	2M	3	9
F2	4F	5	9
F3	4F	4	10
F4	4M	4	10

3.5.2. Potentiodynamic measurements

Tafel polarization curves of uncoated MS and coated MS with the prepared paint formulations in 3.5% NaCl solution are shown in Figure 11. The corrosion kinetic parameters derived from these curves are given in Table 4. A remarkable reduction in the corrosion current density (Icorr) from 0.0001015 A/cm2 for uncoated MS to 2.432E-06 A/cm2 for coat loaded with 3% PAOT on MS (T3). This indicates the effective corrosion protection of the coat contains up to 3% PAOT. The continuous descend of Icorr to 3.78E-07 A/cm2 for zinc-rich PAOT-loaded coats on MS (Z3) demonstrates the role of zinc in the protection of steel through the barrier and cathodic or sacrificial protection, in addition to, the development of patina layer which is a passive, insoluble, and stable film that protects the zinc surface, . An outcome from the figure 11. that there is a clear pitting-corrosion inhibition in case of coats loaded with PAOT which shows very low pitting corrosion in all cases compared to blanks T0, Z0 and F0, this can perfectly comply with the PAOT hypothesis of dispersion of current result from galvanic corrosion cell and hence, cut the electrochemical reaction and prevent corrosion.

3. Conclusion

Plastic emulsion paint was formulated based mainly on synthesized styrene/butyl acrylate, as a binder, and TiO2 as a neutral pigment. To enhance the protection efficiency of the paint coating, TiO2 pigment was replaced by 35.7 % of either zinc phosphate or red ferric oxide as an anticorrosive pigment. Zn3(PO4)2 and Fe2O3 promoted the physical interactions of the coated paint by the chelations originated between the Zn and Fe metals and the lone pair of electrons floating on the polar groups and the aromatic rings of the binder. Moreover, the oxygen atoms in interred in hydrogen bonds with the polar groups of the copolymer. This increased the thermal stability and the

glass transition temperature of the coated paints. The estimation of the steel panels for corrosion after the immersion test showed lower degree of rusting for Zn3(PO4)2 and Fe2O3 than TiO2 coated paints. In order for more enhancement of the protection efficiency, prepared poly (ani-co-o-toluidine), as an inhibitor, was added to the paint formulations by 1%, 2%, 3%, and 4%. The optimum concentration of the inhibitor was found to be 3%. The best paint formula that can be deduced from this study is that loaded with 10% Zn3(PO4)2 (35.7 % of the total pigment amount) and 3% poly (ani-co-o-toluidine).

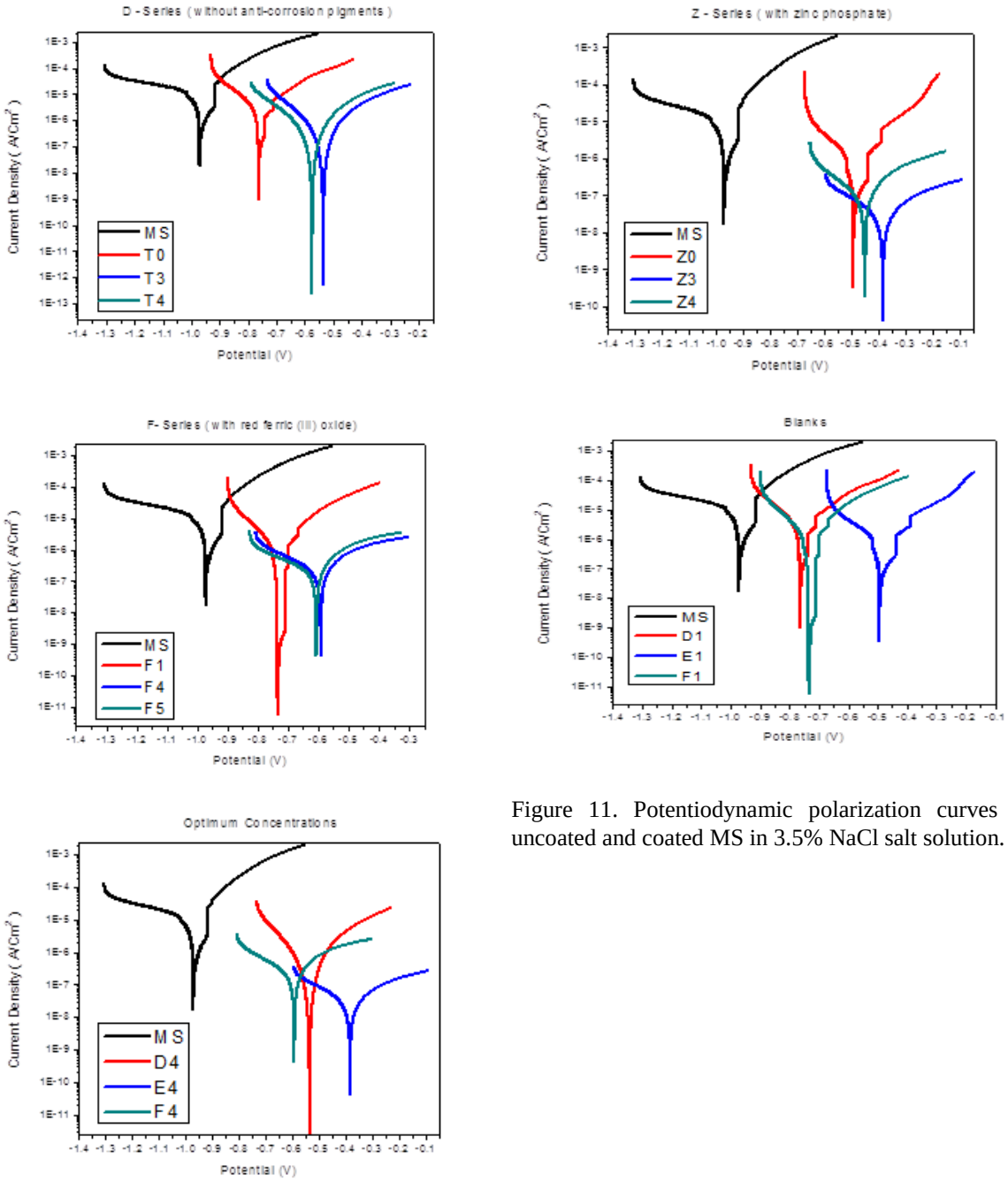

Figure 11. Potentiodynamic polarization curves of uncoated and coated MS in 3.5% NaCl salt solution.

Table 4. Tafel data of coated and uncoated MS samples

Sample Code	βa (mV/dec)	βc (mV/dec)	-Ecorr (mV)	Icorr × 10^7 (A/cm²)	CR × 10^4 (mm/year)	PR (Ω)	Coat efficiency (%)
MS	80.7	350	645	1015	11794	280.58	0
T0	136	122	760	26.4	306.66	10603.38	97.40
T3	198	200	535	3.53	28.256	122312.57	99.65
T4	253	205	572	3.84	45.3	128215.25	99.62
Z0	146	156	476	7.50	87.156	43696.82	99.26
Z3	226	244	380	0.383	4.39	1331926.44	99.96
Z4	117	177	453	0.922	11.3	331028.62	99.91
F0	111	113	734	12.3	142.43	19894.18	98.79
F3	133	219	591	1.25	16.5	287214.53	99.88
F4	96.5	237	605	1.75	2.15	170233.71	99.83

4. References

[1] W. Zhang, H. Yuan, Corrosion fatigue effects on life estimation of deteriorated bridges under vehicle impacts, Engineering Structures, 71 (2014) 128-136.

[2] R.W. Revie, Corrosion and corrosion control: an introduction to corrosion science and engineering, John Wiley & Sons2008.

[3] P.A. Schweitzer, Fundamentals of corrosion: mechanisms, causes, and preventative methods, CRC press2009.

[4] L. Ghasemi- Mobarakeh, M.P. Prabhakaran, M. Morshed, M.H. Nasr- Esfahani, H. Baharvand, S. Kiani, S.S. Al- Deyab, S. Ramakrishna, Application of conductive polymers, scaffolds and electrical stimulation for nerve tissue engineering, Journal of tissue engineering and regenerative medicine, 5 (2011) e17-e35.

[5] C. Li, L. Ding, H. Cui, L. Zhang, K. Xu, H. Ren, Application of conductive polymers in biocathode of microbial fuel cells and microbial community, Bioresource technology, 116 (2012) 459-465.

[6] G. Kaur, R. Adhikari, P. Cass, M. Bown, P. Gunatillake, Electrically conductive polymers and composites for biomedical applications, Rsc Advances, 5 (2015) 37553-37567.

[7] T. Nezakati, A. Seifalian, A. Tan, A.M. Seifalian, Conductive polymers: opportunities and challenges in biomedical applications, Chemical reviews, 118 (2018) 6766-6843.

[8] Y. Shi, L. Peng, Y. Ding, Y. Zhao, G. Yu, Nanostructured conductive polymers for advanced energy storage, Chemical Society Reviews, 44 (2015) 6684-6696.

[9] R. Balint, N.J. Cassidy, S.H. Cartmell, Conductive polymers: Towards a smart biomaterial for tissue engineering, Acta biomaterialia, 10 (2014) 2341-2353.

[10] S.I. Cho, S.B. Lee, Fast electrochemistry of conductive polymer nanotubes: synthesis, mechanism, and application, Accounts of chemical research, 41 (2008) 699-707.

[11] A. Eftekhari, Nanostructured conductive polymers, John Wiley & Sons2011.

[12] A.M. Grancarić, I. Jerković, V. Koncar, C. Cochrane, F.M. Kelly, D. Soulat, X. Legrand, Conductive polymers for smart textile applications, Journal of Industrial Textiles, 48 (2018) 612-642.

[13] S.L. Lee, C.-J. Chang, Recent developments about conductive polymer based composite photocatalysts, Polymers, 11 (2019) 206.

[14] S. Bhadra, D. Khastgir, N.K. Singha, J.H. Lee, Progress in preparation, processing and applications of polyaniline, Progress in polymer science, 34 (2009) 783-810.

[15] K. Lee, S. Cho, S.H. Park, A. Heeger, C.-W. Lee, S.-H. Lee, Metallic transport in polyaniline, Nature, 441 (2006) 65-68.

[16] J. Huang, R.B. Kaner, The intrinsic nanofibrillar morphology of polyaniline, Chemical communications, (2006) 367-376.

[17] Z.A. Boeva, V.G. Sergeyev, Polyaniline: Synthesis, properties, and application, Polymer Science Series C, 56 (2014) 144-153.

[18] X. Zhang, H.S. Kolla, X. Wang, K. Raja, S.K. Manohar, Fibrillar growth in polyaniline, Advanced Functional Materials, 16 (2006) 1145-1152.

[19] P. Humpolicek, V. Kasparkova, P. Saha, J. Stejskal, Biocompatibility of polyaniline, Synthetic metals, 162 (2012) 722-727.
[20] S. Sinha, S. Bhadra, D. Khastgir, Effect of dopant type on the properties of polyaniline, Journal of Applied Polymer Science, 112 (2009) 3135-3140.
[21] A.M. Mohammed, E.S. Shafik, A.I. Hussein, H.A. Derbala, A.K. Elziaty, G.A.E.-m. Elsayed, Synthesis of 2-Alkylbenzimidazole moiety as a novel antioxidant and its effect on physico-mechanical and electrical properties of acrylonitrile butadiene rubber, Egyptian Journal of Chemistry, 63 (2020) 20-21.
[22] A.S. A53/A53M-12, Standard specification for pipe, steel, black and hot-dipped, zinc-coated, welded and seamless, ASTM International West Conshohocken, PA, 2012.
[23] S. Morsi, M. abd El-Aziz, R. Morsi, A. Hussain, Polypyrrole-coated latex particles as core/shell composites for antistatic coatings and energy storage applications, Journal of Coatings Technology and Research, 16 (2019) 745-759.
[24] M. Stern, A method for determining corrosion rates from linear polarization data, Corrosion, 14 (1958) 60-64.
[25] S.M. Morsi, H.S. Emira, S.M. El- Sawy, R.M. Mohsen, L.A. Khorshed, Synthesis and characterization of kaolinite/polyaniline nanocomposites and investigating their anticorrosive performance in chlorinated rubber/alkyd coatings, Polymer Composites, 40 (2019) 2777-2789.
[26] S. Morsi, L. Khorshed, G. Samaan, S. Sobhi, E. Abadir, A. Ismael, Polyaniline emulsion as a passivator in styrene-acrylate waterborne coatings for the protection of carbon steel against corrosion, Egyptian Journal of Chemistry, 62 (2019) 2093-2107.
[27] T.o.c. DIN EN ISO 8044.
[28] R. Mohsen, S. Mohamed, Y. Abu-ayana, A. Ghoneim, Synthesis of Conductive Cu-core/Ag-subshell/polyaniline-shell Nanocomposites and their Antimicrobial Activity, Egyptian Journal of Chemistry, 61 (2018) 939-952.
[29] S. Morsi, R. Mohsen, M. Selim, H. Elsherif, Sol-gel, Hydrothermal, and Combustion Synthetic Methods of Zinc Oxide Nanoparticles and Their Modification with Polyaniline for Antimicrobial Nanocomposites Application, Egyptian Journal of Chemistry, 62 (2019) 1131-1144.
[30] A. Amin, H.M. Darweesh, A.M. Ramadan, S.M. Morsi, M.M. Ayoub, Modification of cement with succinic anhydride- based hyperbranched polyesteramide, Journal of applied polymer science, 124 (2012) 1483-1489.